Nonclassical Nucleation in a Solid-Solid Transition of Confined Hard Spheres

Weikai Qi (齐维开),[1,2] Yi Peng (彭毅),[3] Yilong Han (韩一龙),[3] Richard K. Bowles,[2] and Marjolein Dijkstra[1,*]

[1]*Soft Condensed Matter, Debye Institute for Nanomaterials Science, Department of Physics, Utrecht University,
Princetonplein 5, 3584 CC Utrecht, The Netherlands*
[2]*Department of Chemistry, University of Saskatchewan, Saskatoon, Saskatchewan S7N 5C9, Canada*
[3]*Department of Physics, Hong Kong University of Science and Technology, Clear Water Bay, Hong Kong, China*

A solid-solid phase transition of colloidal hard spheres confined between two planar hard walls is studied using a combination of molecular dynamics and Monte Carlo simulation. The transition from a solid consisting of five crystalline layers with square symmetry (5□) to a solid consisting of four layers with triangular symmetry (4△) is shown to occur through a nonclassical nucleation mechanism that involves the initial formation of a precritical liquid cluster, within which the cluster of the stable 4△ phase grows. Free-energy calculations show that the transition occurs in one step, crossing a single free-energy barrier, and that the critical nucleus consists of a small 4△ solid cluster wetted by a metastable liquid. In addition, the liquid cluster and the solid cluster are shown to grow at the planar hard walls. We also find that the critical nucleus size increases with supersaturation, which is at odds with classical nucleation theory. The △-solid-like cluster is shown to contain both face-centered-cubic and hexagonal-close-packed ordered particles.

The kinetics of phase transitions plays an important role in condensed-matter physics and materials science. In order to gain a better fundamental understanding of how to control self-assembly processes in the fabrication of novel structures, many experimental and simulation studies have been devoted to colloidal systems. Experiments [1–4] and computer simulations [5–7] on bulk hard-sphere colloids suggested that the metastable fluid crystallizes and super-heated crystals melt via a single-step nucleation process that is well described by classical nucleation theory (CNT) [8]. However, Ostwald's step rule suggests that the kinetic pathway to the most stable state can initially proceed through the nucleation of intermediate, metastable phases [9]. The effect of a nearby metastable state on nucleation and the occurrence of multistep nucleation processes have been studied in the crystallization of a range of systems including colloids [10,11], proteins [12], and patchy particles [13], and in the crystallization of molecular solids from solution [14].

In contrast, the kinetic processes of solid-solid phase transitions, which involve complex structural rearrangements [15], have received considerably less attention [16]. Solid-solid transitions usually occur in a martensitic fashion [17,18] involving the concerted, diffusionless motion of the atoms in the unit cell. Anisotropic stress, rapid quenching, and a small system size have been found to promote martensitic transformations [19]. In colloids, martensitic transitions have been observed in small crystalline clusters [20–22] or lattices stretched by external fields [18,23–25]. A solid-solid transition involving an activated nucleation process has recently been experimentally observed at the single-particle level for the first time in colloidal thin-film

crystals confined between two glass plates [26]. The equilibrium phase diagram of hard spheres confined between two planar hard walls shows an alternating sequence of solid-solid transitions, $\dots n\triangle \rightarrow (n+1)\square \rightarrow (n+1)\triangle\dots$, as the plate separation increases [27–30], where n is the number of crystalline layers. Peng *et al.* [26] found that the transition from the $(n+1)\square$ crystal to the $(n)\triangle$ crystal followed Ostwald's step rule and occurred via a two-step nucleation process involving an intermediate liquid phase.

We study the nucleation mechanism of the $5\square \rightarrow 4\triangle$ solid-solid transition in a system of hard spheres of diameter σ confined between two parallel hard plates separated by a distance $H/\sigma = 4$, using computer simulations. Our simulations are carried out in the packing fraction range $0.479 < \eta < 0.500$ (i.e., the 2D reduced lateral pressure range $35.8 < P^* = \beta P \sigma^2 < 40$), where the $5\square$ crystal and the liquid phase are metastable with respect to the $4\triangle$ crystal (see the Supplemental Material [31] for details). The free energy of the liquid phase lies between the free energies of the two solid phases. $\beta = 1/(k_B T)$ denotes the inverse temperature, with T being the temperature and k_B being the Boltzmann constant. In order to explore the role a metastable liquid phase might play in this solid-solid transition, we calculate the free energy of formation for a cluster containing N_L liquidlike particles and $N_\triangle$ solidlike particles with triangular symmetry. The resulting free-energy surface shows that the optimal kinetic pathway for the transition entails the initial growth of a liquid cluster, within which the △-solid cluster forms, but there is only one nucleation barrier involving a critical cluster consisting of liquid- and solidlike particles in our parameter regime.
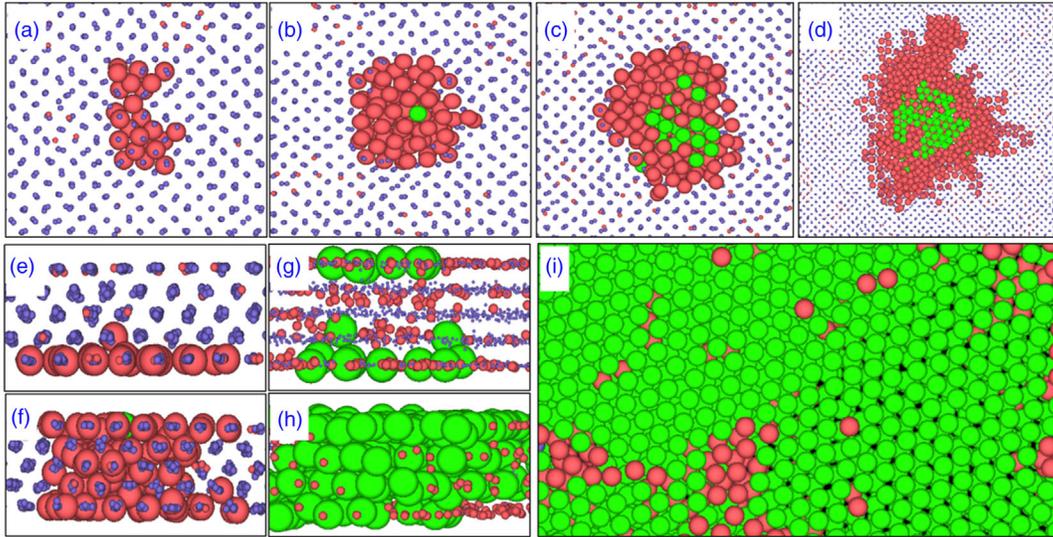
FIG. 1 (color online).   Typical configurations of the solid-solid transition. Configurations obtained by umbrella sampling in MC simulations with a bias towards cluster sizes of (a) $N_{\rm cl} = 60$, (b) $N_{\rm cl} = 120$, and (c) $N_{\rm cl} = 180$ particles. (d) A configuration obtained by EDMD simulation at $t = 518\tau$ for $\eta = 0.490$. Side (e) and top (f) views of a liquid nucleus in an EDMD simulation. Side (g) and top (h) views of a $\triangle$-solid nucleus in an EDMD simulation. (i) A solid consisting of four $\triangle$ layers arranged in both fcc and hcp structures from EDMD simulations. In (a)–(d), multilayer particles are projected onto the xy plane. $\square$-solid, $\triangle$-solid and liquidlike particles are colored in blue, green, and red, respectively. Particles not belonging to the largest cluster are drawn small.

To distinguish between fluidlike and solidlike particles with square ($\square$) and triangular ($\triangle$) symmetries, we calculate the bond orientational order $\psi_{mj} = \sum_{k=1}^{N_b(j)} \exp{(im\theta_k)}/N_b(j)$ of each particle j with $m = 4, 6$ for solidlike particles with four- and sixfold symmetries, where θ_j is the angle between the bond of particles i and j with an arbitrary reference axis, and $N_b(j)$ denotes the number of nearest neighbors of particle j [34]. We divide the system into five and four layers for the calculation of ψ_4 and ψ_6, respectively. In addition, a crystalline bond with m-fold symmetry is defined if $|\psi_{mi}^* \cdot \psi_{mj}| > 0.5$ [26]. We define particles as $\triangle$-solid-like if the number of crystalline bonds with triangular symmetry $\xi_\triangle \geq 3$, and as $\square$-solid-like if the number of crystalline bonds with square symmetry $\xi_\square \geq 2$. All other particles are defined as liquidlike. The criteria guarantee that no particle is both $\square$-solid-like and $\triangle$-solid-like. Liquid- and $\triangle$-solid-like particles are considered to belong to the same cluster if the distance between any two particles is less than 1.5σ.

We perform Monte Carlo (MC) simulations using the umbrella sampling technique in the isothermal-isobaric (NPT) ensemble, with the number of particles $N = 2000$, the reduced 2D lateral pressure $P^* = 40$, and the temperature T fixed. Figure 1(a)–1(c) show typical configurations along the nucleation pathway in MC simulations. Nucleation studies usually focus on a one-dimensional free-energy barrier using the total cluster size, $N_{\rm cl}$, as the reaction coordinate. Hence, we calculate the free energy, $\beta\Delta G(N_{\rm cl}) = -\log \mathcal{P}(N_{\rm cl})$, where $\mathcal{P}(N_{\rm cl})$ is the probability of observing a cluster of size $N_{\rm cl} = N_L + N_\triangle$.

We use two different biasing potentials: $W(N_{\rm cl}) = \frac{1}{2}k(N_{\rm cl} - N_{\rm cl0})^2$ and $W(N_L) = \frac{1}{2}k(N_L - N_{L0})^2$. The first biasing potential is designed to follow the growth of a binary cluster and the second the possible nucleation of a liquid cluster, but we stress that the potential does not prevent the growth of $\triangle$-solid-like particles. $N_{\rm cl0}$ and N_{L0} are the umbrella window centers for the total cluster size and the number of liquid particles in the cluster, respectively. The sampling is performed using 60 umbrella centers, equally spaced in the region $N_{\rm cl}, N_L \in [0, 300]$. For each umbrella window, the data are harvested from 10000 equilibrium configurations and averaged over ten independent runs. The free energies from each umbrella window are combined into a single curve using the multistage Bennet acceptance ratio method [35].

Figure 2 shows that the two biasing schemes give similar free energies for cluster sizes up to $\sim$100, where the cluster consists solely of liquidlike particles [Figs. 1(a) and 1(b)]. At larger cluster sizes, the two free-energy curves begin to diverge with the emergence of $\triangle$-solid-like particles in the $N_{\rm cl}$ biasing scheme but not in the N_L biasing scheme, which suggests a degree of hysteresis. If both schemes were fully equilibrated, we would expect them to yield similar free energies, but the newly emerged $\triangle$-solid particles are not easily sampled when the N_L biasing potential is employed. $N_\triangle$ increases rapidly for both biasing schemes at the free-energy maximum, where $N_{\rm cl}^* \sim 175$, but Fig. 2(b) also shows that $N_\triangle$ is already increasing, even before the maximum under $N_{\rm cl}$ biasing.

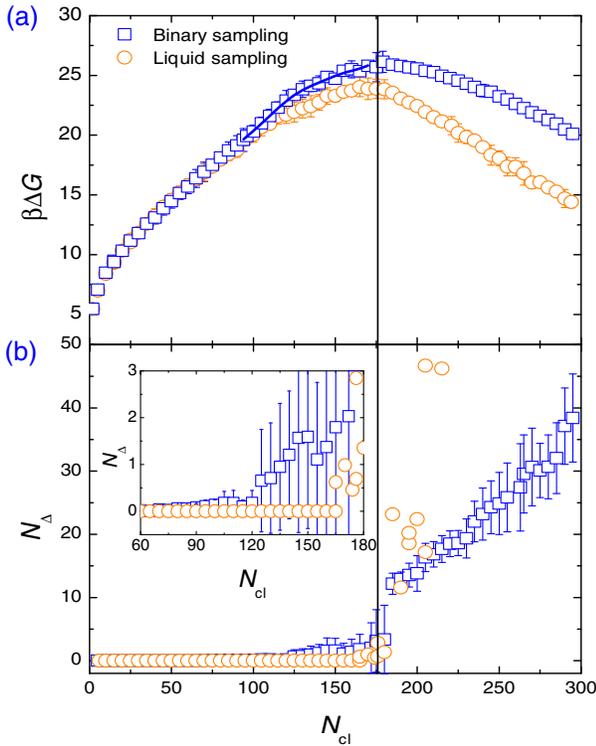More insight into the nucleation mechanism can be obtained by calculating the two-dimensional free-energy

FIG. 2 (color online). (a) The Gibbs free energy $\Delta G(N_{cl})/(k_B T)$ as a function of the total number of particles N_{cl} using the $W(N_{cl})$ biasing potential (the squares) and the $W(N_L)$ biasing potential (the circles). (b) Number of $\triangle$-like particles $N_\triangle$ averaged over 10000 nuclei as a function of cluster size N_{cl} as obtained from the two biasing methods. (Inset) The same plot as (b) but with the region $60 < N_{cl} < 180$ enlarged for clarity. The vertical line marks the critical nucleus size.
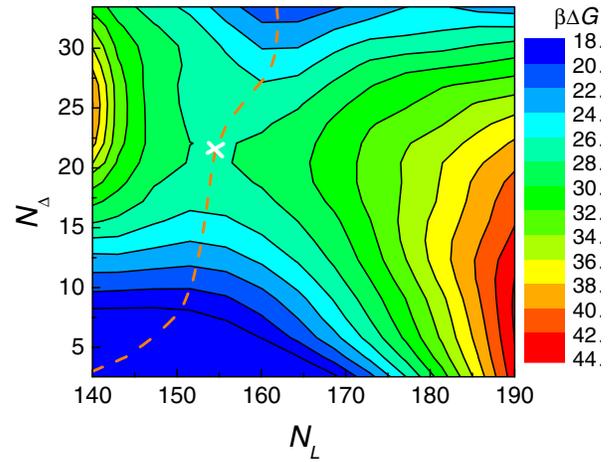

FIG. 3 (color online). Contour plot of $\beta\Delta G(N_L, N_\triangle)$ in the saddle point region. The nucleation barrier height $\beta\Delta G^* \approx 26$ and the critical cluster (the white cross) contains $N_L = 155$ liquidlike particles and $N_\triangle = 22$ $\triangle$-solid-like particles. The lowest free-energy path through the saddle point region is indicated by the dashed orange curve.

surface of forming a cluster containing N_L and $N_\triangle$ particles, $\beta\Delta G(N_L, N_\triangle) = -\log P(N_L, N_\triangle)$, where $P(N_L, N_\triangle)$ denotes the probability of observing the largest cluster in the system with $(N_L, N_\triangle)$. We perform MC simulations using umbrella sampling in the NPT ensemble, at the same thermodynamic conditions, and use a quadratic biasing potential, $W(N_L, N_\triangle) = \frac{1}{2}[k_L(N_L - N_{L0})^2 + k_\triangle(N_\triangle - N_{\triangle 0})^2]$ [36], where $\beta k_L = 0.15$ and $\beta k_\triangle = 0.3$. A total of 300 umbrella windows are used, with adjacent umbrella window centers separated by five particles, covering the ranges $N_{L0} \in [0, 250]$ and $N_{\triangle 0} \in [0, 30]$. For each umbrella window, the system is equilibrated for 10^7 MC steps before data are collected over the next 2×10^6 MC steps, harvesting configurations every 200 MC steps. We present the contour plot of the free-energy surface in the $N_L - N_\triangle$ plane in Fig. 3. We see a significant increase in the free energy of growing pure liquidlike clusters beyond $N_L \approx 170$, and we do not find a saddle point leading to the nucleation of the pure liquid phase. Instead, the lowest free-energy path on the surface shows that a $\triangle$-solid-like cluster starts growing inside the pre-critical liquid cluster and that the critical embryo contains

$N_\triangle \approx 25$ solidlike particles surrounded by $N_L \sim 155$ liquidlike particles [Fig. 1(c)]. Beyond the nucleation saddle point, the new phase continues to grow as $N_\triangle$ and N_L both increase [Fig. 1(d)]. A key feature of our free-energy surface is the presence of a single free-energy barrier leading to the $\triangle$ crystal, which suggests that the transition occurs in a single step, even though a liquid cluster is developed in the initial stages of the nucleation process. The free-energy surface has a similar form to that obtained by ten Wolde and Frenkel [12] in their study of protein crystallization. They showed that the lowest free-energy path proceeds via the formation of a liquidlike droplet, within which a crystallite starts to form.

A simple CNT for our system, where the nucleus has a cylindrical core of $\triangle$-solid particles surrounded by a layer of liquid particles, exhibits a two-step mechanism (see Fig. S6). A saddle point associated with a pure liquid critical cluster leads to the liquid free-energy basin, which is then separated from the $\triangle$-crystal basin by a ridge on the free-energy surface, so nucleation requires the crossing of two barriers. Accounting for the disjoining pressure [37,38] associated with the thin wetting layer and the strain energy of the lattice [15], the CNT introduces a saddle point on the free-energy surface with a liquid-$\triangle$-solid critical cluster leading directly to the crystal phase, as observed in our simulations, but the valley floor approaching this saddle point, and hence the precritical fluctuations, grows along the $\triangle$-solid axis. In our simulation results, the early stages of nucleation are characterized by the formation of pure liquidlike clusters, which is at odds with CNT.

Finally, we use event-driven molecular dynamics (EDMD) simulations in the canonical (NVT) ensemble to obtain the dynamics of the nucleation process, starting
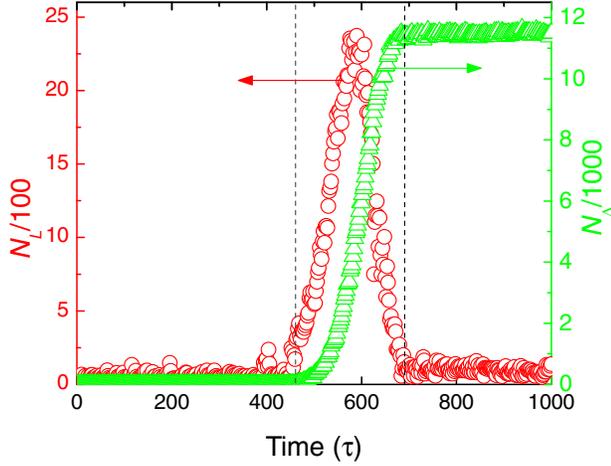
FIG. 4 (color online). The number of liquidlike particles (left), N_L, and $4\triangle$ like particles (right), $N_\triangle$, in the largest cluster as a function of time t in MD time units.
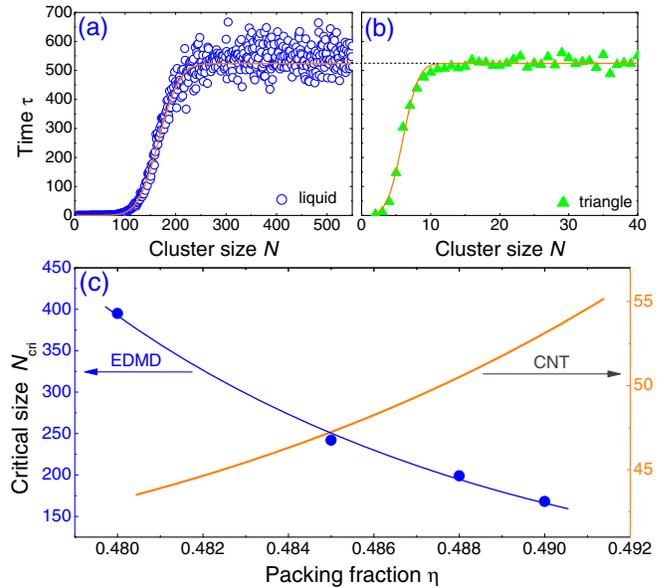

FIG. 5 (color online). The mean first passage time $\tau(N)$ for (a) liquid and (b) $4\triangle$ clusters in EDMD simulations at $\eta = 0.490$. Lines are fits of the mean first passage time using $1/C_1\{1 + \mathrm{erf}[C_2(N - N_{\mathrm{cri}})]\}$ where erf is the error function [40,41]. For liquid clusters, $C_1 = 0.00382$, $C_2 = 0.02161$, and $N_{\mathrm{cri}} = 167$. For $4\triangle$ clusters, $C_1 = 0.00382$, $C_2 = 0.39442$, and $N_{\mathrm{cri}} = 6$. (c) The critical size of the liquid nucleus as a function of the packing fraction calculated from the fitting of the mean first passage time in EDMD simulations (the blue dots) and classical nucleation theory (the orange line) (see the Supplemental Material [31], Sec. III).

from a metastable defect-free $5\square$ phase. At $\eta \geq 0.5$ (i.e., $P^* \geq 40$ in the $5\square$ phase), the EDMD runs never nucleate on the time scale of our simulations. Nucleation events begin when η is reduced to 0.49. A long induction period is observed during which the liquid cluster size fluctuates and the number of $N_\triangle$ remains near zero (Fig. 4). The initial liquid cluster appears to form at the hard-wall interface in a heterogeneous fashion [Fig. 1(e)]. It then grows into a cylindrical nucleus spanning the two walls [Fig. 1(f)]. The $\triangle$-solid cluster forms within the fluctuating liquid also at the liquid-wall interface [Fig. 1(g)], which is consistent with studies of the prefreezing and crystallization of the bulk hard-sphere fluid at a hard-wall interface [39]. In our EDMD simulations, the number of liquid particles N_L surges to a maximum before decreasing as the liquid is consumed in the growth of the $\triangle$-nucleus [Figs. 1(h) and 4], which contains either face-centered-cubic (fcc) or hexagonal-close-packed (hcp) layering [Fig. 1(i)].

To further examine the possibility that the liquid and the $\triangle$ crystal nucleate independently of each other, we estimate the nucleation rate by measuring the mean first passage time, $\tau(N)$, during the appearance of a cluster containing $N = N_L$ or $N = N_\triangle$ particles [40,41] (see the Supplemental Material [31] for more details). Figures 5(a) and 5(b) show that the mean first passage times for the liquid and the $\triangle$ solid reach their plateaus at similar times, yielding a nucleation rate $J = C_1/(2V) = 1.43 \times 10^{-7}\tau/\sigma^3$, where V is the sample volume. At a lower η, the liquid nucleates slightly slower than the solid (see Table II in the Supplemental Material [31]), which indicates that the $\triangle$ solid nucleates within a precritical liquid nucleus. Furthermore, the critical nucleus size is determined from the EDMD simulations as a function of η. According to CNT, the critical size of the liquid nucleus should decrease as η decreases (i.e., as the chemical potential difference between the liquid and the $5\square$ crystal

increases). However, Fig. 5(c) shows the opposite trend: the number of liquid particles in the critical cluster actually increases. A possible explanation for this unconventional finding might be that the liquid clusters correspond to precritical fluctuations with a correlation length that increases as the limit of stability of the $5\square$ crystal is approached with respect to the liquid [12,42] (i.e., upon lowering the packing fraction η).

Solid-solid transitions usually occur through a martensitic process when the driving force for nucleation is small and the barrier is high because it avoids the need to develop a solid-solid interface, which has a high free-energy cost. However, our simulations show that the $5\square \rightarrow 4\triangle$ solid-solid transition occurs via a nonclassical nucleation mechanism involving an intermediate liquid stage. This provides an alternative mechanism that also obviates the need to form a solid-solid interface. Furthermore, the initial nuclei should always be liquid if the $\triangle - \square$ interfacial free energy is higher than the sum of the $\triangle$-liquid and liquid-$\square$ interfacial free energies since the interfacial free energy dominates over the bulk chemical potential difference when the nucleus is small enough. Since the mechanism is general, intermediate liquids could exist widely in other systems. For example, the interfacial energy in metals and alloys ranges from 500 to $1000 \sim \mathrm{mJ/m^2}$ for the incoherent

interfaces between two crystalline phases and from 30 to $250 \sim mJ/m^2$ for solid-liquid interfaces [15]. Hence, an intermediate liquid stage could similarly exist in the solid-solid transformation of metals.

*M.Dijkstra1@uu.nl

[1] K. Schätzel and B. J. Ackerson, Phys. Rev. Lett. **68**, 337 (1992).

[2] B. J. Ackerson and K. Schätzel, Phys. Rev. E **52**, 6448 (1995).

[3] U. Gasser, E. R. Weeks, A. Schofield, P. N. Pusey, and D. A. Weitz, Science **292**, 258 (2001).

[4] Z. Wang, F. Wang, Y. Peng, Z. Zheng, and Y. Han, Science **338**, 87 (2012).

[5] S. Auer and D. Frenkel, Nature (London) **409**, 1020 (2001).

[6] L. Filion, M. Hermes, R. Ni, and M. Dijkstra, J. Chem. Phys. **133**, 244115 (2010).

[7] T. Kawasaki and H. Tanaka, Proc. Natl. Acad. Sci. U.S.A. **107**, 14036 (2010).

[8] D. Turnbull and J. C. Fisher, J. Chem. Phys. **17**, 71 (1949).

[9] W. Ostwald, Z. Phys. Chem. (Leipzig) **22**, 289 (1897).

[10] H. J. Schöpe, G. Bryant, and W. van Megen, Phys. Rev. Lett. **96**, 175701 (2006).

[11] P. Tan, N. Xu, and L. Xu, Nat. Phys. **10**, 73 (2014).

[12] P. R. ten Wolde and D. Frenkel, Science **277**, 1975 (1997).

[13] L. O. Hedges and S. Whitelam, J. Chem. Phys. **135**, 164902 (2011).

[14] D. Erdemir, A. Y. Lee, and A. S. Myerson, Acc. Chem. Res. **42**, 621 (2009).

[15] D. A. Porter, K. E. Easterling, and M. Y. Sherif, *Phase Transformations in Metals and Alloys* (CRC Press, Boca Raton, FL, 2002).

[16] U. Gasser, J. Phys. Condens. Matter **21**, 203101 (2009).

[17] A. G. Khachaturyan, *Theory of Structural Transformation in Solids* (John Wiley & Sons, New York, 1983).

[18] A. Yethiraj, A. Wouterse, B. Groh, and A. van Blaaderen, Phys. Rev. Lett. **92**, 058301 (2004).

[19] R. Z. Khaliullin, H. Eshet, T. D. Kühne, J. Behler, and M. Parrinello, Nat. Mater. **10**, 693 (2011).

[20] M. T. Casey, R. T. Scarlett, W. B. Rogers, I. Jenkins, T. Sinno, and J. C. Crocker, Nat. Commun. **3**, 1209 (2012).

[21] I. C. Jenkins, M. T. Casey, J. T. McGinley, J. C. Crocker, and T. Sinno, Proc. Natl. Acad. Sci. U.S.A. **111**, 4803 (2014).

[22] J. A. Weiss, D. W. Oxtoby, D. G. Grier, and C. A. Murray, J. Chem. Phys. **103**, 1180 (1995).

[23] S. Nojd, P. S. Mohanty, P. Bagheri, A. Yethiraj, and P. Schurtenberger, Soft Matter **9**, 9199 (2013).

[24] Y. Yang, L. Fu, C. Marcoux, J. E. S. Socolar, P. Charbonneau, and B. B. Yellen, Soft Matter **11**, 2404 (2015).

[25] P. S. Mohanty, P. Bagheri, S. Nöjd, A. Yethiraj, and P. Schurtenberger, Phys. Rev. X **5**, 011030 (2015).

[26] Y. Peng, F. Wang, Z. Wang, A. M. Alsayed, Z. Zhang, A. G. Yodh, and Y. Han, Nat. Mater. **14**, 101 (2015).

[27] P. Pieranski, L. Strzelecki, and B. Pansu, Phys. Rev. Lett. **50**, 900 (1983).

[28] M. Schmidt and H. Löwen, Phys. Rev. Lett. **76**, 4552 (1996).

[29] S. Neser, C. Bechinger, P. Leiderer, and T. Palberg, Phys. Rev. Lett. **79**, 2348 (1997).

[30] A. Fortini and M. Dijkstra, J. Phys. Condens. Matter **18**, L371 (2006).

[31] See Supplemental Material at http://link.aps.org/supplemental/10.1103/PhysRevLett.115.185701, which includes Refs. [32,33], for phase behavior, CNT model and nucleation rate calculations.

[32] K. Zahn and G. Maret, Phys. Rev. Lett. **85**, 3656 (2000).

[33] A. Härtel, M. Oettel, R. E. Rozas, S. U. Egelhaaf, J. Horbach, and H. Löwen, Phys. Rev. Lett. **108**, 226101 (2012).

[34] D. R. Nelson, *Defects and Geometry in Condensed Matter Physics* (Cambridge University Press, Cambridge, England, 2009).

[35] M. R. Shirts and J. D. Chodera, J. Chem. Phys. **129**, 124105 (2008).

[36] S. Auer and D. Frenkel, J. Chem. Phys. **120**, 3015 (2004).

[37] Y. S. Djikaev, R. Bowles, H. Reiss, K. Hämeri, A. Laaksonen, and M. Väkevä, J. Phys. Chem. B **105**, 7708 (2001).

[38] M. Iwamatsu, J. Chem. Phys. **134**, 164508 (2011).

[39] M. Dijkstra, Phys. Rev. Lett. **93**, 108303 (2004).

[40] J. Wedekind, R. Strey, and D. Reguera, J. Chem. Phys. **126**, 134103 (2007).

[41] S. E. M. Lundrigan and I. Saika-Voivod, J. Chem. Phys. **131**, 104503 (2009).

[42] R. Ni, S. Belli, R. van Roij, and M. Dijkstra, Phys. Rev. Lett. **105**, 088302 (2010).